Int. J. Heat Mass Transfer. Vol. 35, No. 6, pp. 1573–1587, 1992
Printed in Great Britain

0017–9310/92 $5.00 + 0.00
Pergamon Press Ltd

Experimental study of transient natural convection of glycerol–water mixtures in a side heated cavity

C. G. JEEVARAJ and JOHN C. PATTERSON
Centre for Water Research, University of Western Australia, Nedlands, WA 6009, Australia

(*Received* 16 *August* 1990 *and in final form* 11 *January* 1991)

Abstract—Results of a series of experiments performed in a square cavity suddenly heated and cooled on opposing sidewalls are reported. The initially stationary and isothermal working fluid is in all cases a glycerol–water mixture giving a variation in Prandtl number over the range 13–234. This range, together with a variation in the end to end temperature difference, allows exploration of the parameter space in which the transition from a monotonic to an oscillatory approach to steady state is predicted by the classification scheme of Patterson and Imberger (*J. Fluid Mech.* **100**, 65–86 (1980)). The results confirm the classification, and other aspects of the flow development, including the characteristics of the growth of the thermal boundary layers, and some characteristics of the horizontal intrusions from the thermal layers into the cavity.

INTRODUCTION

IN RECENT years the investigation of transient natural convection in cavities with differentially heated sidewalls has led to some understanding of the manner in which the flow and heat transfer evolves from an initial condition to a steady state. In particular, the case of a rectangular cavity containing an initially isothermal (at temperature T_0) and quiescent fluid suddenly heated and cooled on the opposing sidewalls to temperatures $T_0 \pm \Delta T$ has received considerable attention since the scaling and numerical analysis of this problem by Patterson and Imberger [1]. They devised a classification scheme to describe the various regimes of the flow, which depended on the value of the Rayleigh number (Ra) relative to various combinations of the other parameters influencing the flow, i.e. the Prandtl number (Pr) and the aspect ratio (A), where

$$Ra = \frac{g\alpha\Delta T h^3}{\nu\kappa}$$

$$Pr = \frac{\nu}{\kappa}$$

$$A = \frac{h}{L}. \qquad (1)$$

According to ref. [1], the flow ultimately evolved into one of conductive, convective, or transitional steady states, classified by $Ra < 1$, $Ra > \max(Pr^2, A^{-12})$, and $1 < Ra < \max(Pr^2, A^{-12})$, respectively. Within each of these broad flow regimes, however, a number of sub-regimes also existed, which described the manner in which the flow evolved. In general, these characterized the time, length and velocity scales of the developing motion. Seven such regimes were shown to exist, and numerical results were used to test the validity of the flow descriptions. At that time, however, no experimental results were available to test the scaling.

Of particular interest in the convective regime $Ra > \max(Pr^2, A^{-12})$ was the prediction that the net heat transfer across the cavity approached steady state as a decaying oscillation. This had also been observed numerically by, e.g. Gresho *et al.* [2] and Staehle and Hahne [3]. For the case $Pr > A^{-6}$, the following regimes are relevant [1]:

Regime III: $\max(Pr^2, A^{-12}) < Ra < Pr^4 A^{-4}$, in which the oscillatory heat transfer behaviour is not expected, the approach to steady state is monotonic and the horizontal motions are governed by a viscous–buoyancy balance.

Regime IV: $Pr^4 A^{-4} < Ra < Pr^{10}$, in which the approach to a steady-state heat transfer is oscillatory, but the characteristics of the motions are similar to Regime III.

Regime V: $Pr^{10} < Ra < Pr^{16} A^{-12}$, in which the approach is also oscillatory, but the motions are influenced by inertial effects.

Regime VI: $Pr^{16} A^{-12} < Ra$, in which the approach is oscillatory, but the horizontal motions are governed by an inertia–buoyancy balance.

The first experiment to specifically examine the transient behaviour following sudden heating and cooling of the sidewalls was that of Yewell *et al.* [4]. Although designed to test for the presence of the oscillatory approach to steady state, these experiments were actually in a regime in which the oscillations were not expected and, consistent with this, were not observed. Notwithstanding this result, and the relatively slow start-up of the experiment, Patterson [5] showed that

NOMENCLATURE

A	aspect ratio
C_p	specific heat [J kg^{-1} C^{-1}]
g	acceleration due to gravity [m s^{-2}]
h	cavity height [m]
L	cavity length [m]
N	Brunt–Väisälä frequency [s^{-1}]
Pr	Prandtl number
Q	two-dimensional fluid flux [m^2 s^{-1}]
Ra	Rayleigh number
t	time [s]
T_0	initial temperature [°C]
T_v	intrusion passage time [s]
ΔT	temperature increase and decrease [°C]
v	boundary layer velocity scale [m s^{-1}]
y	height [m].

Greek symbols

α	coefficient of thermal expansion [°C^{-1}]
$\delta(y)$, δ_t	thermal boundary layer thickness [m]
Δ_{in}	intrusion thickness [m]
κ	thermal diffusivity [m^2 s^{-1}]
ν	kinematic viscosity [m^2 s^{-1}]
τ	thermal boundary layer time scale [s]
ω	internal wave frequency [s^{-1}].

their results were entirely consistent with the classification of ref. [1]. Ivey [6] carried out a series of experiments also designed to test for the existence of the oscillatory behaviour. Here, the correct regime was selected, with $Ra \sim 10^9$, $Pr \sim 7$ in a cavity of aspect ratio 1, and evidence of oscillatory behaviour was expected. The results did not, however, give a clear indication of the regular, first mode internal wave oscillations expected; however, there were indications of a much higher frequency signal which appeared to be associated with the downstream behaviour of the horizontal intrusions from the corners, interpreted by Ivey as an internal hydraulic jump.

The properties of these intrusions and the associated high frequency waves have been discussed at length in a numerical context by Paolucci and Chenoweth [7], Schladow *et al.* [8], Schladow [9], and Armfield and Patterson [10]. The apparent conflict between the numerical and existing experimental results with respect to the oscillatory approach to steady state was not resolved until the experimental results of Patterson [11] and the combined numerical and experimental investigation of Patterson and Armfield [12] resulted in the identification of the principal features of the flow development and a description of the associated generation mechanisms for the particular case $Ra = 3.26 \times 10^8$, $Pr = 7.5$, and $A = 1$. This placed the experiment near the boundary of Regimes IV and V, both of which are expected to show clear evidence of the oscillatory behaviour.

The conclusions of that study are reported in the cited literature; in the present context it is sufficient to note that the scaling given in ref. [1] for the particular combination of parameters was supported, and that the high frequency signals observed in ref. [6] and numerically in refs. [7, 9] and Armfield [13] were identified as instabilities appearing at two separate instances in the thermal boundary layer, associated firstly with the start-up and secondly with the impact of the first intrusion on the opposing boundary layer. Schladow [9] and Armfield and Patterson [10] have discussed these aspects at length, for the particular Ra in question. The experimental results confirmed, for the first time, the presence of the first mode internal wave activity during the flow development.

In spite of this interest in the development of these flows, the Patterson [11] and Patterson and Armfield [12] experiment remained the only documented observations of the unsteady problem which was consistent with the numerical results. The observations were also consistent with the scaling and classification of ref. [1], but with only a single point in the parameter space, the results were still open to question. The numerical results were also limited in scope, dealing with a limited range of the parameter space. The recent paper of Hyun and Lee [14], which also supported much of the scaling, extended this range somewhat, however, the deficiency in the experimental results remained.

In the present paper the results of a series of experiments using the equipment described in refs. [11, 12] are reported. In this series, mixes of glycerol and water with various compositions were used, together with the full range of temperature differences possible in the present apparatus, to alter both Pr and Ra so that the experiments ranged from the upper part of Regime III to the lower part of Regime V. The relevance of the model of ref. [1] for the transient flow in Regimes III and IV is verified, and the important features of the flow developments are identified. In particular, the presence of an oscillatory approach to steady state in Regimes IV and V, and its absence in Regime III, is confirmed, consistent with the classification given in ref. [1]. Further, with the aid of comprehensive thermistor time series, a number of key aspects of the scaling analysis are quantified. These data are supplemented by streak photographs which give a qualitative view of the characteristics which distinguish the various regimes.

EXPERIMENTAL PROCEDURES

The experimental apparatus and the measurement techniques were similar to those described in refs.

[11, 12], and will be described only briefly here. The working fluid is contained in a 24 cm square cavity of width 50 cm, the end walls, top and base of which are constructed from 19 mm perspex sheeting. The vertical hot and cold side walls are made from braced 1 mm copper sheet. Insulated hot and cold water baths are separated from the copper walls by a 3 cm air gap; the bath walls facing the copper walls are pneumatically controlled gates which rise vertically in a fraction of a second. Thus on initiation, the gates rise and the bath water floods against the copper walls. The bath temperatures were controlled to within 0.03°C. The combination of the rapid start-up with the high thermal inertia of the baths gives a close approximation to the required step function boundary condition. To prevent heat leakage, a sheet of polystyrene foam is placed in the air gap during the experimental set-up, to be removed prior to the initiation of the experiment. The base, lid, and end walls are also insulated, with one end wall insulation being removable for photography.

Temperature data were obtained with Thermometric fast response FP07 thermistors located at various points in the cavity as described below. The thermistors were inserted through the cavity lid and were sampled by a 12 bit A–D board. After preamplification, the resolution of the temperature signal was 0.007°C. The signal was sampled at 2 Hz, sufficiently fast to resolve all expected frequencies. The thermistors were positioned with the aid of a travelling microscope which had a resolution of 0.1 mm. However, the thermistor beads are of $O(1\text{ mm})$ in size, and the measurements are therefore integrated over this region. The locations of the thermistors varied from experiment to experiment.

Flow visualization for the streak photographs was achieved with AQ1000 rheoscopic particles (manufactured by Kalliroscope Corporation, Massachusetts, U.S.A.) illuminated by a 1 cm sheet of light in the central plane of the cavity. The streak photographs were taken at f11.0, using Ilford XP1-400 monochrome film, at exposure periods which varied from experiment to experiment. Due to their platelet form, in regions of high shear the particles align their longest dimension in the flow direction, and become less visible. As a result, the photographs are not suitable for the determination of velocities, but give an integrated picture of the flow direction over the exposure period.

The dynamic viscosity and density of the various glycerol–water mixtures used were measured with a Well Brookfield cone viscometer and a DMA60 Paar density meter, respectively. An additional check on these measurements was made with a measurement of the kinematic viscosity with a Cannon–Fenske routine viscometer. The other fluid parameters, α, κ and C_P, were obtained from Segur [15]. Values of the viscosity and density of the actual mixtures used in the experiments are given in Table 1.

Table 1 also shows the other variables for each experiment reported here. In the table, the experiments are identified by the Julian day on which they occurred (e.g. 224). The initial temperature T_0, the temperature difference ΔT, and the values of Pr and Ra are also given in the table. To illustrate the position of the experiments in the parametric domain, the experimental conditions are plotted on a Ra–Pr diagram (Fig. 1). For $A = 1$, as is the case here, the regime boundaries on the log–log diagram are simple straight lines. Thus the upper and lower boundaries of Regime IV are shown on the figure, and each of Regimes III–V are indicated. On the figure, the positions of the experiments are shown, together with the experiments of Ivey [6] and Patterson [11]. The series of experiments ranges from the upper part of Regime III to the lower part of Regime V.

RESULTS AND DISCUSSION

In the following discussion of the results, reference will, in general, be made to the hot wall shown at the right-hand side and to the heated intrusion. As the temperature difference is small, the Boussinesq assumption is assumed, giving symmetry of the flow and temperature fields. The cold wall and cold intrusion will therefore display similar behaviour.

Table 1. Measured values of the dynamic viscosity and density of the glycerol–water mixture and the details of the experimental conditions

Exp. No.	Dynamic viscosity [kg m^{-1} s^{-1}]	Density [kg m^{-3}]	T_0 [°C]	ΔT [°C]	Pr	Ra
224	28.3×10^{-3}	1.192×10^{3}	16.2	1.0	234	2.9×10^{7}
129	10.0×10^{-3}	1.149×10^{3}	19.8	0.5	81	3.3×10^{7}
146	10.4×10^{-3}	1.15×10^{3}	17.2	1.0	84	6.4×10^{7}
156	10.0×10^{-3}	1.149×10^{3}	17.2	2.0	80	1.3×10^{8}
158	8.9×10^{-3}	1.139×10^{3}	17.3	4.5	83	3.4×10^{8}
172	3.4×10^{-3}	1.085×10^{3}	17.15	2.0	29	2.8×10^{8}
181	2.5×10^{-3}	1.068×10^{3}	17.6	2.0	18	3.1×10^{8}
245	2.1×10^{-3}	1.056×10^{3}	17.1	1.0	16	1.6×10^{8}
249	1.8×10^{-3}	1.046×10^{3}	17.3	1.5	13	2.7×10^{8}

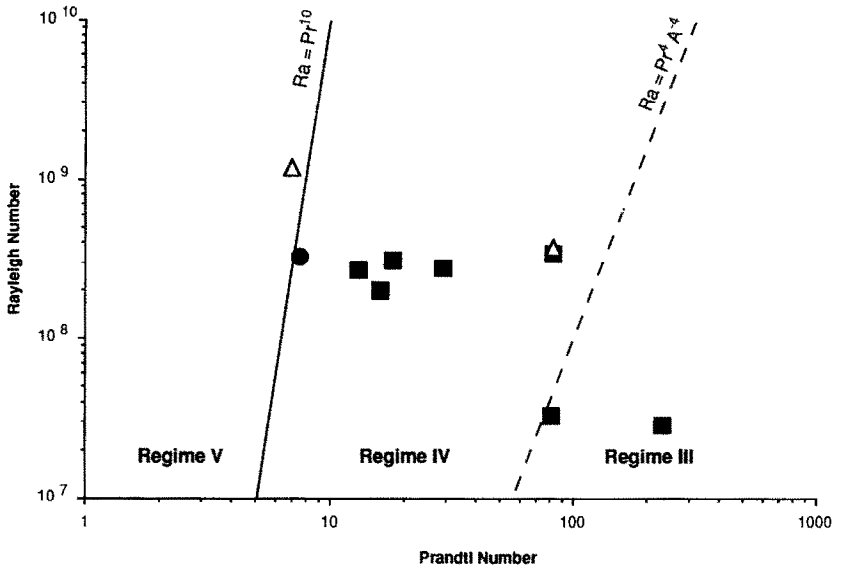

FIG. 1. Rayleigh number–Prandtl number diagram showing the location of the present transient experiments: ■, for aspect ratio = 1; △, Ivey [6]; ●, Patterson [11].

Thermal boundary layer

For $Ra > Pr^2$, ref. [1] showed that the steady-state boundary layer thickness scale δ_T was given by

$$\delta_T \sim \frac{h}{Ra^{1/4}} \tag{2}$$

occurring after a time scale τ

$$\tau \sim \frac{h^2}{\kappa\, Ra^{1/2}} \tag{3}$$

with a vertical velocity scale v

$$v \sim \frac{\kappa\, Ra^{1/2}}{h}. \tag{4}$$

These steady-state scales represent a balance between the conduction of heat in through the boundary and the convection of heat away. According to ref. [1], steady state was preceded by a balance between buoyancy and viscosity, and between temperature increase and conduction; the boundary layer grew as a purely conductive layer until time τ.

For the purposes of a qualitative description of the boundary layer growth over the range of the experiments, not all of the experiments are fully reported here. In Figs. 2(a)–(d) time series are shown from the thermistors placed in the thermal boundary layer in four experiments (224, 172, 181 and 249, respectively) which span the entire experimental range. The actual locations of the thermistors are shown in the inset on each figure.

The temperature signals in all cases show essentially the same basic characteristics; an initial period in which the temperature is essentially unchanged, a period of exponential growth, and an approximately constant signal which may be influenced by oscillations at the change from exponential growth and at a later stage. According to the model of refs. [1, 12], the initial period of no signal corresponds to the time required for the conduction of heat from the boundary to increase the temperature at the thermistor location to the resolution of the thermistor, which is then followed by a period in which the boundary layer responds simply to thermal conduction. According to Brown and Riley [16], this period continues until a singularity generated by the start-up (referred to as the leading edge effect) moves from the lowest point up the hot wall. At each vertical position, the balance changes from conduction–unsteady temperature to conduction–vertical convection as the singularity passes. If the thermal boundary layer thickness is increased beyond its steady-state value then the passage of the singularity will be accompanied by a travelling wave crest and, if the boundary layer is unstable, a trailing wave train that increases in amplitude in the direction of travel. The Brown and Riley analysis also assumed that the wave travels at the peak velocity in the boundary layer.

Figure 2(a) shows the result for experiment 224 ($Ra = 2.9 \times 10^7$, $Pr = 234$). As shown in Fig. 1, the experiment is located well within Regime III. On the basis of the stability analysis of Gill and Davey [17], a travelling wave is not expected for this high Prandtl number case. The signal clearly shows the exponential growth followed by a period of approximately steady state, with no wave activity. Experiment 172 ($Ra = 2.8 \times 10^8$, $Pr = 29$) is well inside Regime IV. Figure 2(b) shows that a weak effect is present at the end of the exponential growth period, followed by evidence of very weak oscillatory behaviour at approximately 160 s, following impact from the incoming cold intrusion. Figure 2(c) shows the result

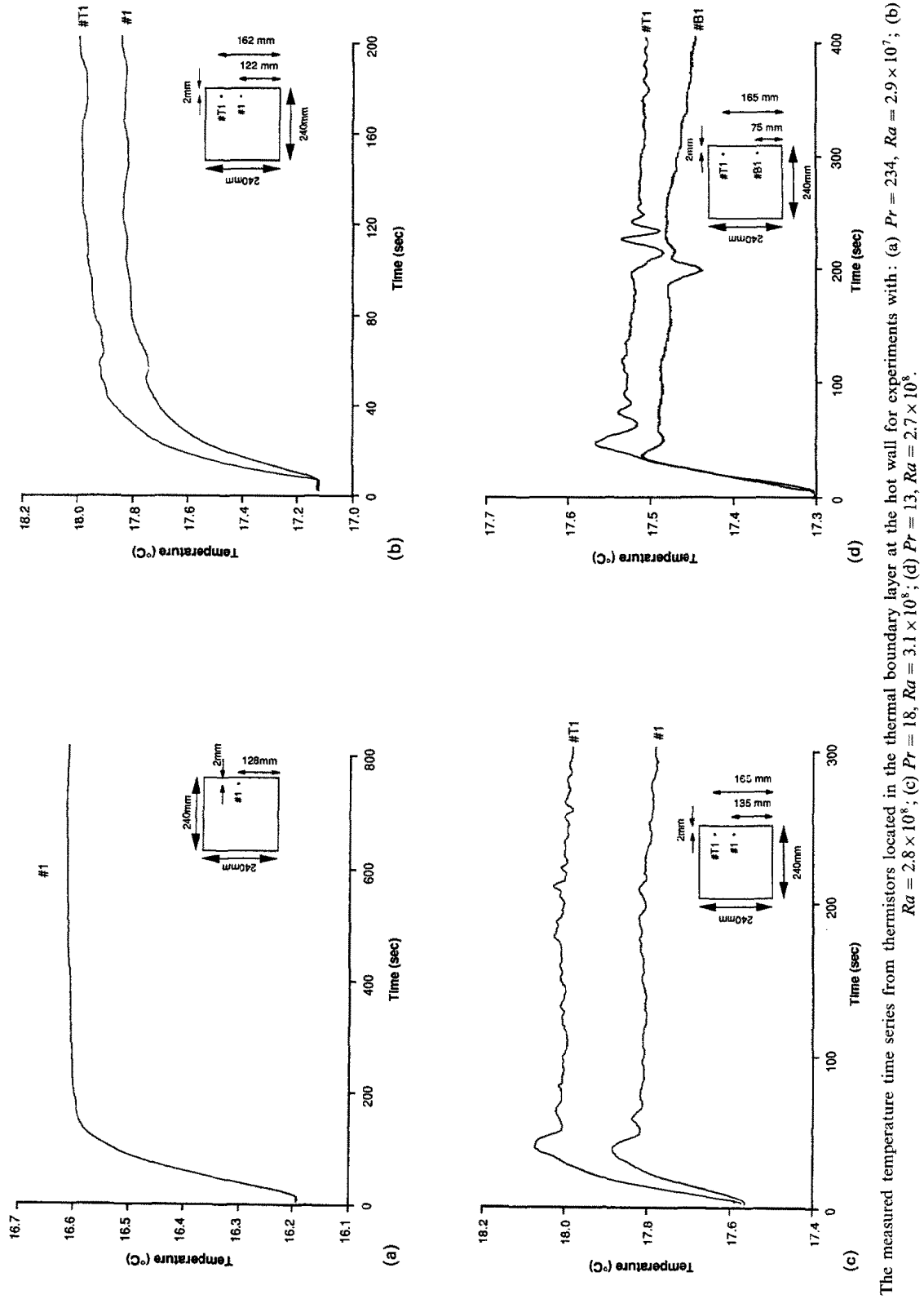

FIG. 2. The measured temperature time series from thermistors located in the thermal boundary layer at the hot wall for experiments with: (a) $Pr = 234$, $Ra = 2.9 \times 10^7$; (b) $Pr = 29$, $Ra = 2.8 \times 10^8$; (c) $Pr = 18$, $Ra = 3.1 \times 10^8$; (d) $Pr = 13$, $Ra = 2.7 \times 10^8$.

for experiment 181 ($Ra = 3.1 \times 10^8$, $Pr = 18$). In this case the initial instability is clearly visible following the exponential growth period, and the secondary instability is again only weakly present. Figure 2(d) (experiment 249; $Ra = 2.7 \times 10^8$, $Pr = 13$) shows a clear indication of both groups of instabilities, and is similar in character to the results reported by refs. [9, 10, 12]. In this case, the experiment is positioned near the upper boundary of Regime IV.

For the Regime III case (Fig. 2(a)), the travelling waves are also not present following the impact of the intrusion. This is evidently related to the relatively increased viscosity. It is plausible to suggest that the increased viscous boundary layer, of thickness $O(Pr^{1/2}\delta_T)$, which lies outside the thermal layer, acts as a buffer to prevent the impact of the incoming intrusion on the thermal layer. As mentioned earlier, the absence of the travelling waves can also be related to the stable boundary layer according to the stability analysis of ref. [17]. The presence or otherwise of the leading edge effect is dealt with in some detail for related problems by Williams *et al.* [18], and a discussion is beyond the scope of this paper, except to note that a direct interpretation of the Williams *et al.* results suggests that for a uniform temperature on a semi-infinite vertical wall, a temperature overshoot, corresponding to the passage of the leading edge effect, is expected, for low Pr values. On the other hand, the results of Goldstein and Briggs [19] suggest that the presence of an overshoot is strongly dependent on the value of Pr, with overshoot becoming undershoot with increasing Pr, consistent with the results observed here.

The data presented here may be used for comparison with the growth time scale for the boundary layer, given by equation (3) [1], modified by the description of the layer ahead of the travelling wave as a purely horizontal conduction layer [16]. Since the wave travels at the maximum speed of the layer, the thermal layer will be of non-uniform thickness. The scaling given in ref. [1] may be modified to give a scaling for the thickness at height y, as follows.

The layer thickness is now a function of position y. Thus, ahead of the travelling wave

$$\delta_T^2(y) \sim \kappa t \tag{5}$$

reflecting a growing conduction layer. The motion is driven by a balance between buoyancy and viscous forces

$$v\frac{v(y)}{\delta_T^2(y)} \sim g\alpha\Delta T \tag{6}$$

and growth continues until convection and conduction balance

$$v\frac{\Delta T}{y} \sim \kappa\frac{\Delta T}{\delta_T^2(y)}. \tag{7}$$

The balance in equation (7) is identical to that obtained by considering the passage of the instability to height y with velocity v, i.e. the Brown and Riley [16] scale.

The solution of equations (5)–(7) then yields

$$\tau(y) \sim \frac{h^{3/2}y^{1/2}}{\kappa\, Ra^{1/2}} \tag{8}$$

and a net flux of heated fluid in the thermal boundary layer of

$$Q \sim \kappa\, Ra^{1/4} \tag{9}$$

identical to the result given in ref. [1].

The scale for the time to steady state of the boundary layer at height y given by equation (8) may be tested with the experimental data, including that contained in Figs. 2(a)–(d). Figure 3 shows the values of

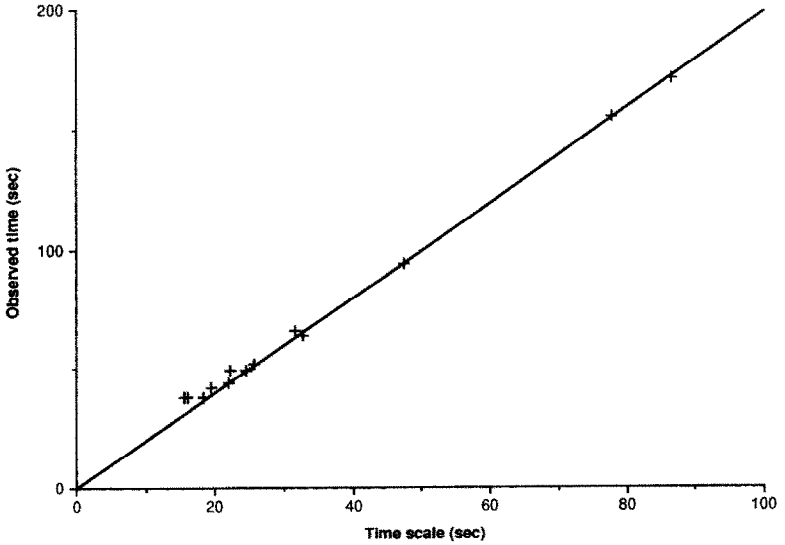

FIG. 3. A plot of observed time for the thermal boundary layer to reach steady state against the time scale, $h^{3/2}y^{1/2}\kappa^{-1}\,Ra^{-1/2}$, to verify equation (8).

the times at which the exponential growth period is estimated from the data to be complete, plotted as a function of $h^{3/2}y^{1/2}\,Ra^{-1/2}\,\kappa^{-1}$, using all of the data. In those cases where oscillatory behaviour was clearly visible, the time was estimated as that when the temperature signal reached the first maximum, i.e. the passage of the first wave. For those cases which approached the steady value without oscillation, the time was estimated as that for which the measured temperature had reached 0.95 of the steady value. The figure shows an excellent straight line fit to the data, providing strong support to the scaling of equation (8). The actual relationship suggested by the data is

$$\tau(y) = 2.0\left[\frac{h^{3/2}y^{1/2}}{\kappa\, Ra^{1/2}}\right]. \tag{10}$$

Horizontal intrusions and flow evolution

The presence of the upper boundary forces the heated fluid to discharge from the thermal boundary layer into the cavity in a heated intrusion along the insulated upper boundary, driven by the horizontal baroclinic pressure gradient. For $Ra < Pr^{10}$, ref. [1] showed that the intrusion was governed by an inertia–buoyancy balance initially, becoming viscous before traversing the cavity width. The intrusion passage time was estimated in ref. [1] as

$$T_v \sim \frac{h^2}{\kappa\, Ra^{7/16}} \tag{11}$$

with final thickness

$$\Delta_{vf} \sim \frac{h}{Ra^{3/16}}. \tag{12}$$

These scales are expected to be relevant for all of the experiments reported here, based on the classification given in ref. [1].

The behaviour of the intrusions is discussed in the context of time series data from a number of thermistors placed along the cavity lid, and from streak photographs taken at various times throughout the flow development. In all cases, the hot wall is on the right, and the streaks are taken over the times indicated in the text and in the legends.

Five thermistors were placed 15 mm below the cavity upper boundary, at horizontal locations 5, 8.5, 12 (mid-point), 15.5 and 19 cm from the hot wall. When the hot intrusion reaches a thermistor, it is registered by a sudden rise in temperature. Thus the data from the five thermistors give an estimate of the intrusion speed. As the thickness of the intrusion depends on the properties of the working fluid and the Ra value, the position of the thermistors relative to the intrusion boundary changes in each experiment. Thus the shape of the temperature signal cannot be compared from experiment to experiment, and only a qualitative comparison can be made.

Figure 4(a) (experiment 224; $Ra = 2.9 \times 10^7$, $Pr = 234$) shows a typical result for the experiments located in Regime III. A gradual, smooth rise is registered by all thermistors as the intrusion passes by, indicating a total absence of the instabilities mentioned above. The streak photographs from this experiment (Figs. 4(b), 0–40 s; 4(c), 120–160 s; 4(d), 900–940 s) give a clear picture of the development of the flow from initiation. Heated fluid from the thin thermal boundary layer emerges from the upper right corner, and unheated fluid from the viscous boundary layer discharges into the core region as a potential flow (Fig. 4(b)). A closed circulation forms beneath the horizontal intrusion, and meets with the corresponding circulation from the cold wall, yielding a slightly tilted central core rotation (Fig. 4(c)). A divergence away from the horizontal wall is also evident. The mechanism responsible for this is discussed in ref. [12], although the divergence here is considerably less rapid than that observed at higher Ra. At later times however, the divergence has evidently vanished (Fig. 4(d)), and a weak reverse flow is observed, splitting the intrusion into a thin stream which travels along the upper boundary and an inner stream which is deflected towards the core region. This flow reversal and splitting of the intrusion was commented on in detail by Patterson and Armfield [12], and held responsible for the generation of the cavity scale seiching observed, and for the stratification of the core.

Figure 5 details the corresponding results for experiment 172 ($Ra = 2.8 \times 10^8$, $Pr = 29$). This experiment is located well inside Regime IV. Here, the characteristic shape shows evidence of the passage of the nose of the intrusion as it passes by each thermistor. In the previous case, the thermistor was evidently contained well within the intrusion and the passage of the nose was recorded as a simple rise in temperature. In this case the thermistor registers a rise followed by a fall, as the nose passes, indicating that the thermistor is much closer to the intrusion boundary. The shape of the time series from the thermistor closest to the hot wall is different to that recorded by the other thermistors. This thermistor is located upstream of the intrusion flow divergence discussed below, and is influenced by a much narrower intrusion. Thus the nose signal shows less of a peak as it passes by. There is no evidence of the travelling waves which were weakly evident on the boundary layer thermistors. These have apparently dissipated by the time the signal reaches the horizontal measuring stations.

The streak photographs for this case are shown in Figs. 5(b)–(d). These are of similar character to the previous set, with greatly amplified features; the flow divergence near the emergent corner of the intrusion is clearly evident in Fig. 5(b), together with the formation of a closed counter clockwise eddy beneath the emerging intrusion. The divergence is much sharper than in the previous case, and has the appearance of the higher Ra case observed in ref. [12]. The eddy ultimately moves in towards the centre of the cavity to meet with its counterpart from the cold wall,

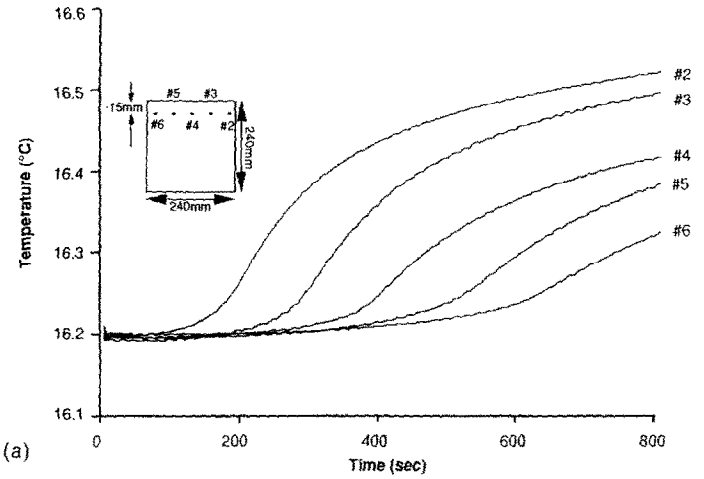

FIG. 4(a). The measured temperature time series at thermistor locations #2 #6 for experiment 224 ($Ra = 2.9 \times 10^7$, $Pr = 234$).

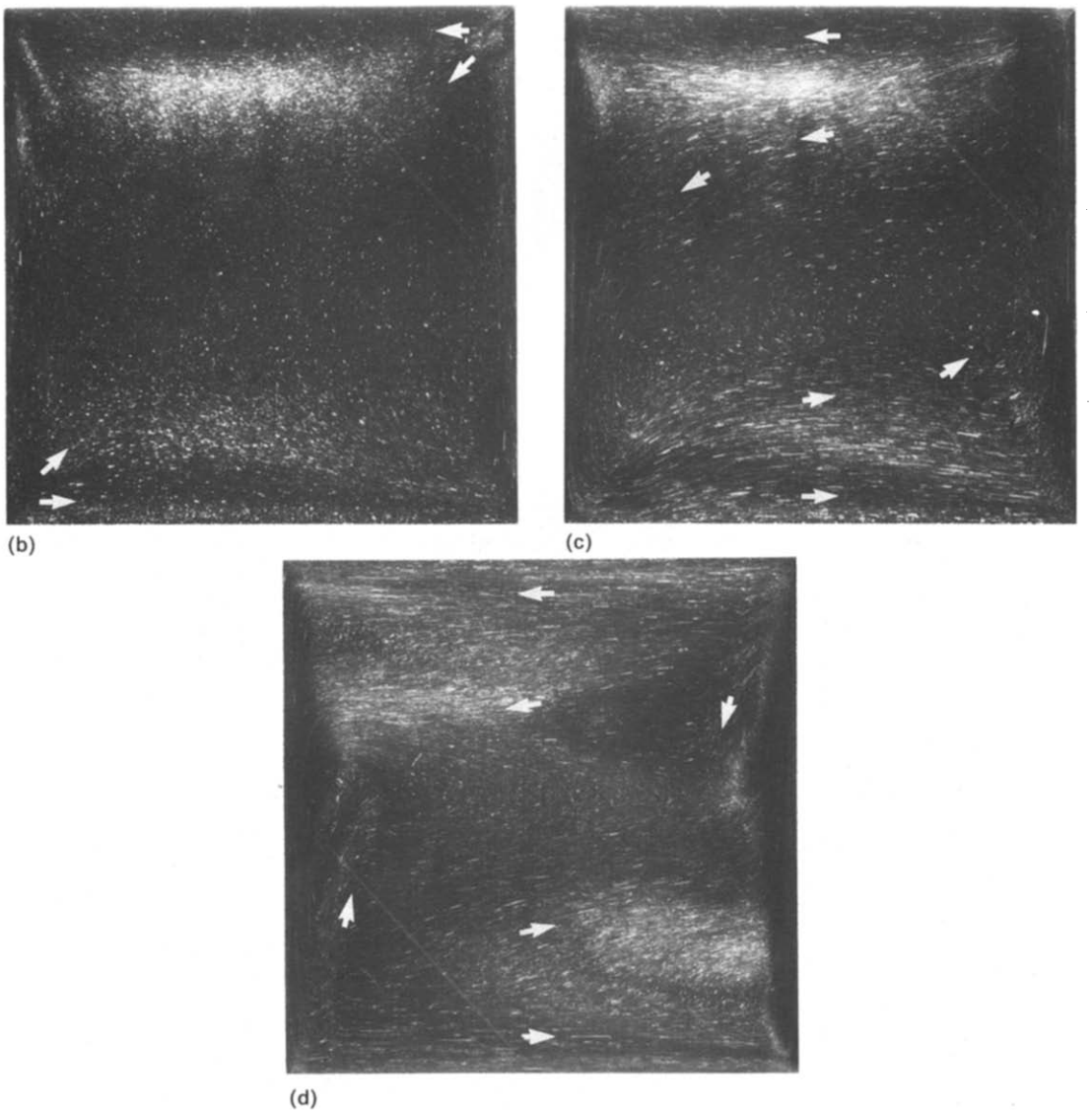

FIGS. 4(b)–(d). Streak photographs of the transient flow for experiment 224. Photographs are exposed for 40 s starting at times (in seconds): (b) 0; (c) 120; (d) 900.

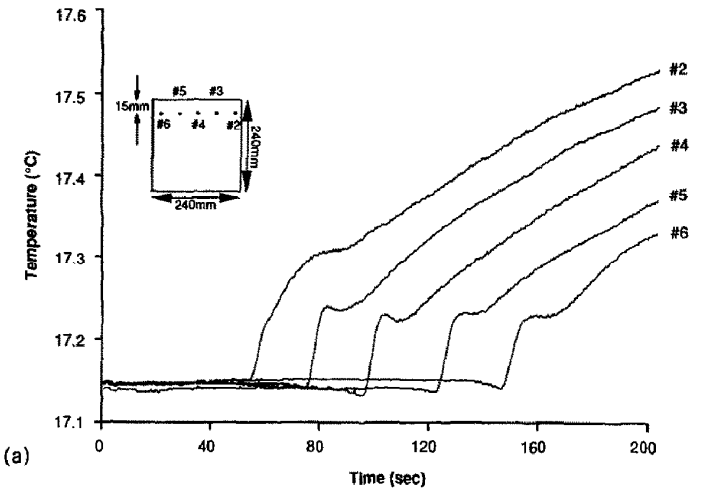

FIG. 5(a). The measured temperature time series at thermistor locations #2–#6 for experiment 172 ($Ra = 2.8 \times 10^8$, $Pr = 29$).

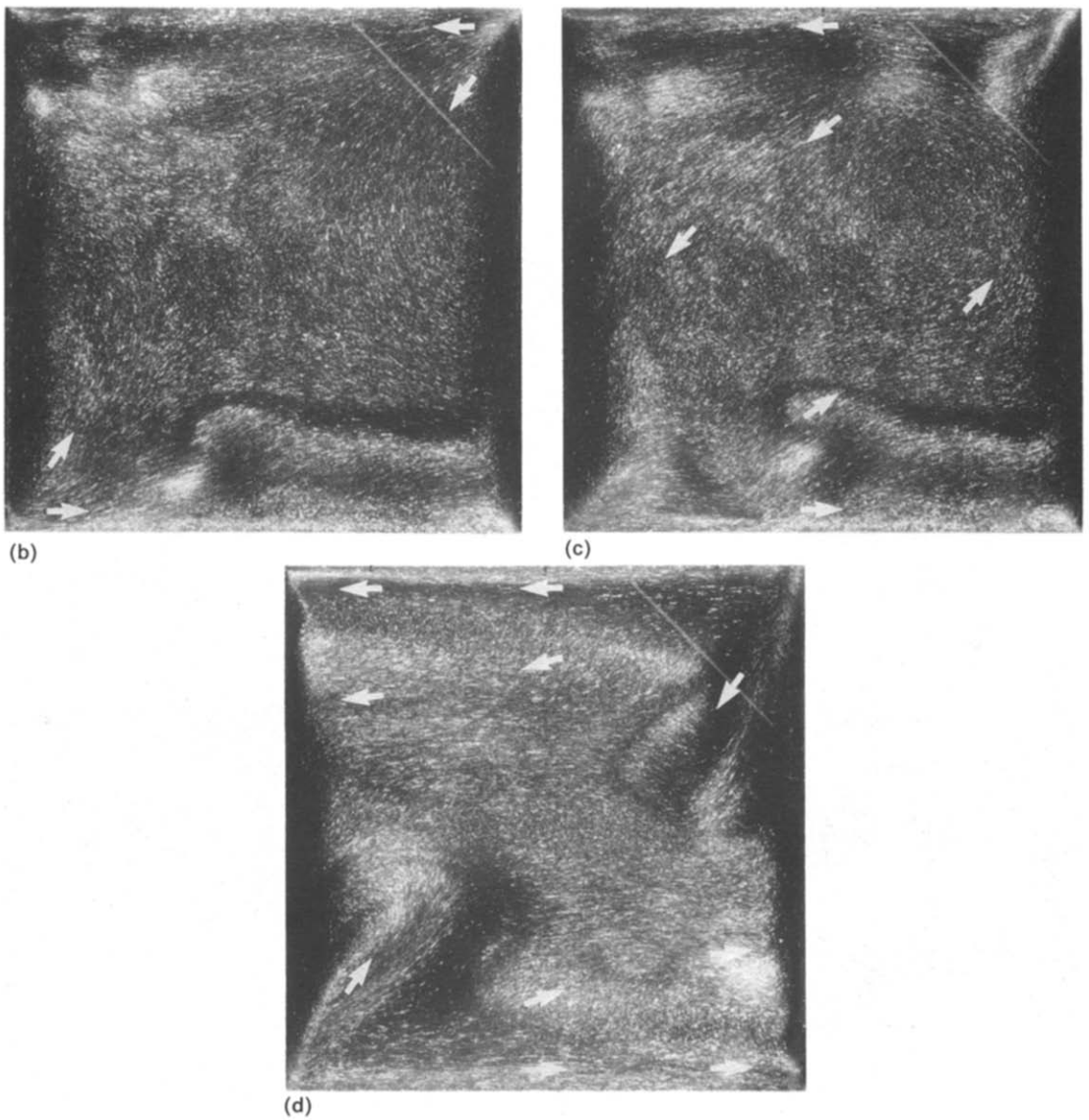

FIGS. 5(b)–(d). Streak photographs of the transient flow for experiment 172. Photographs are exposed for 16 s starting at times (in seconds): (b) 40; (c) 80; (d) 320.

to form a strongly rotating tilted central core (Fig. 5(c)). The tilting of the core is evidently due to the reverse flow observed in the intrusion as in the previous case, although much stronger for this Ra Pr combination. The reverse flow splits the incoming intrusion, forcing a major part of the heated intrusion to be deflected down towards the centre of the cavity (Fig. 5(d)).

Experiment 249 falls in the upper part of Regime IV, and the features of the previous case are expected to be even more strongly present. Figure 6(a) shows the thermistor signals in the intrusion; again the passage of the nose is clearly evident, and again the character of the first thermistor is substantially different to the remainder as the result of its location upstream of the flow divergence. Additional signals are present in these records however, in the form of an oscillatory component on two separate occasions. The first, immediately following the nose, corresponds to the passage of the travelling wave generated by the initiation of the thermal boundary layer, as discussed above in the context of Fig. 2(d). The amplitude of the signal decreases rapidly with passage along the cavity lid, indicating that, although the signal is a genuine instability in the thermal boundary layer, the horizontal layer is stable. The second group of oscillations, evident at approximately 250 s, is the result of the intrusion from the cold wall striking the base of the hot thermal boundary layer. The resultant perturbation, also observed on Fig. 2(d), dies away quickly with passage along the intrusion, again demonstrating that the layer is stable. The development

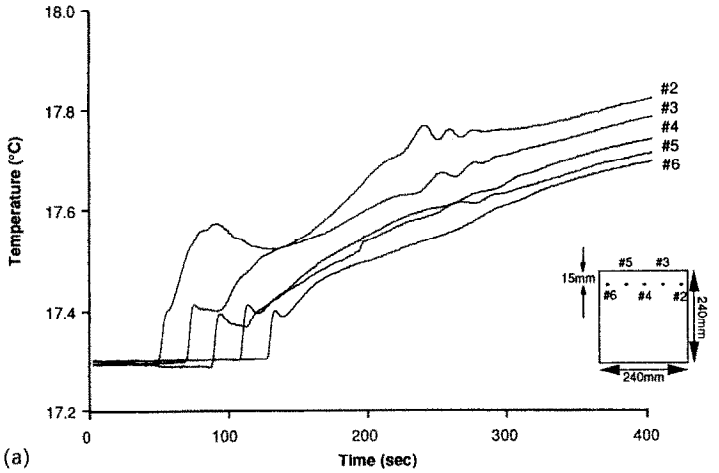

FIG. 6(a). The measured temperature time series at thermistor locations #2–#6 for experiment 249 ($Ra = 2.7 \times 10^8$, $Pr = 13$).

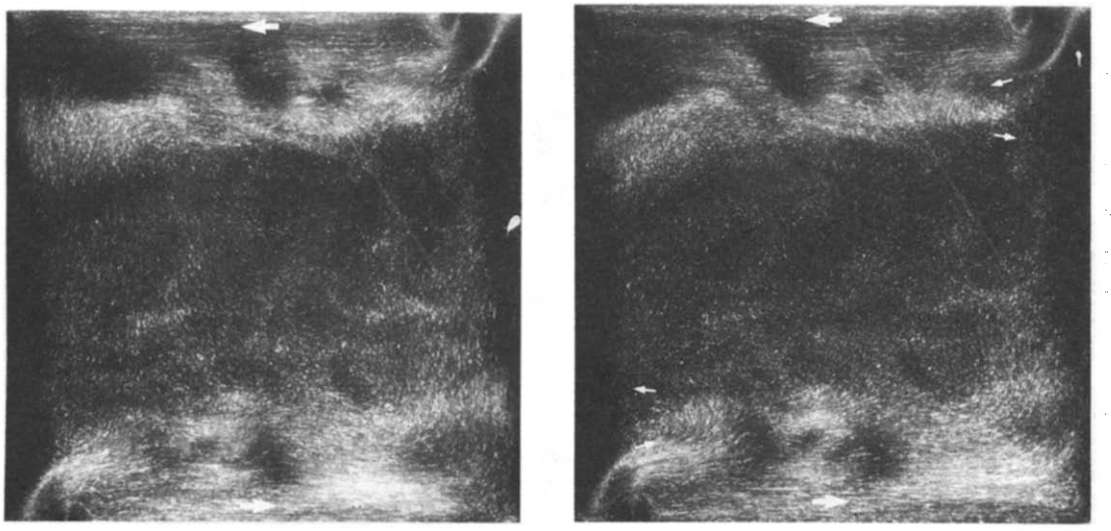

FIGS. 6(b) and (c). Streak photographs of the transient flow for experiment 249. Photographs are exposed for 20 s starting at times (in seconds): (b) 210; (c) 240.

of the flow is similar to experiment 172, and only two streak photographs are shown (Figs. 6(b) and (c)). These show the formation of the counterclockwise eddy beneath the intrusion at the emergent corner (Fig. 6(b)) which again ultimately forms the core flow, and the splitting of the intrusion and consequent tilting of the lower intrusion stream (Fig. 6(c)). The flow divergence near the emergent corner is strongly accentuated, and becomes re-attached to the horizontal boundary shortly downstream, with a region of recirculation evident immediately downstream of the divergence. The properties of the emergent flow appear to have been substantially modified by the flow reversal and the consequent rocking of the structure.

These experiments span Regime IV, and the streak photographs clearly show that the character of the flow changes drastically as the Ra value increases, although the same general features are present. At high Pr and low Ra, the intrusion is relatively thick, the flow divergence is distributed over the full cavity width, and the intrusion splitting, although present, does not modify the conditions at the emergent corner. With increasing Ra and decreasing Pr, however, the intrusion narrows, the divergence becomes increasingly sharp, and the flow reversal resulting from the splitting of the intrusion penetrates back to the region of the rapid divergence. The experiments of ref. [12] are at the lower bound of Regime V, and show these features even more strongly.

The temperature data may also be used to examine the validity of the intrusion scaling described above in equations (11) and (12). As the times of temperature increase are an indicator of the passage of the intrusion, the velocity of the intrusion nose may be estimated. From equations (9) and (12), the velocity should, for a fully viscous layer, scale with $\kappa Ra^{7/16} h^{-1}$. The observed velocities for all experiments, based on the times of passage of the intrusion nose, are shown in Fig. 7, plotted against $\kappa Ra^{7/16} h^{-1}$. The points corresponding to the experiments with $Pr > 80$, located in Regime III and the lower part of Regime IV lie on a straight line, confirming the scaling for the intrusion in those regimes. Evidently, in the upper part of Regime IV, inertial effects are becoming increasingly important, and the data deviates from the straight line indicated by the purely viscous cases. For all of the cases presented in Fig. 7, a quantitative estimation of the ratio of viscous to inertial forces ranges from 2 to 90. All the results which deviate from the proposed straight line have a ratio less than 10, implying that, although viscous forces may be comparatively larger, the presence of inertial effects cannot be ignored.

Cavity scale seiching

As discussed above, the predicted presence of a decaying oscillatory approach to steady state at least partly motivated the experiments of refs. [4, 6], which did not demonstrate the expected behaviour, as discussed in refs. [5, 8–10]. The experiments described by refs. [11, 12] however did show evidence of these waves, by recording the temperature difference between two locations in the horizontal intrusion, equally spaced about the mid-point. Any cavity scale oscillation should be present at these points, as the node of the first mode wave will be at the mid-point. Thus, the two thermistor signals are expected to be one half period out of phase, and their difference

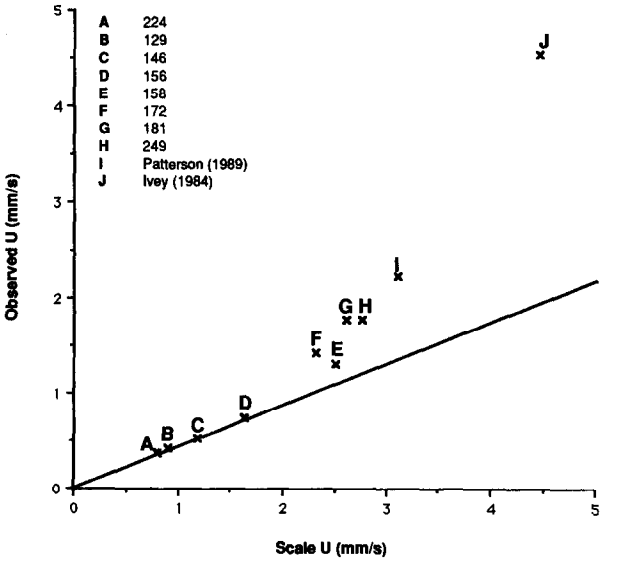

FIG. 7. A plot of observed velocity of the horizontal intrusion against $\kappa Ra^{7/16} h^{-1}$ to verify the velocity scaling derived from equation (11). The solid line indicates that the points corresponding to the experiments with $Pr > 80$ confirm the scaling for the intrusion.

is expected to show clearly the presence of a first mode oscillation. According to the scaling of ref. [1], these oscillations should not be present in Regime III, but should be present in higher regimes, i.e. $Ra > Pr^4 A^{-4}$.

Figure 8(a) shows the temperature difference between the thermistors located at 8.5 and 15.5 cm from the hot wall, for experiment 224 ($Ra = 2.9 \times 10^7$, $Pr = 234$). Located in Regime III, since $Ra < Pr^4 A^{-4}$, the result is expected not to show evidence of waves. Since the waves are generated by the interaction of the incoming intrusions with the far wall

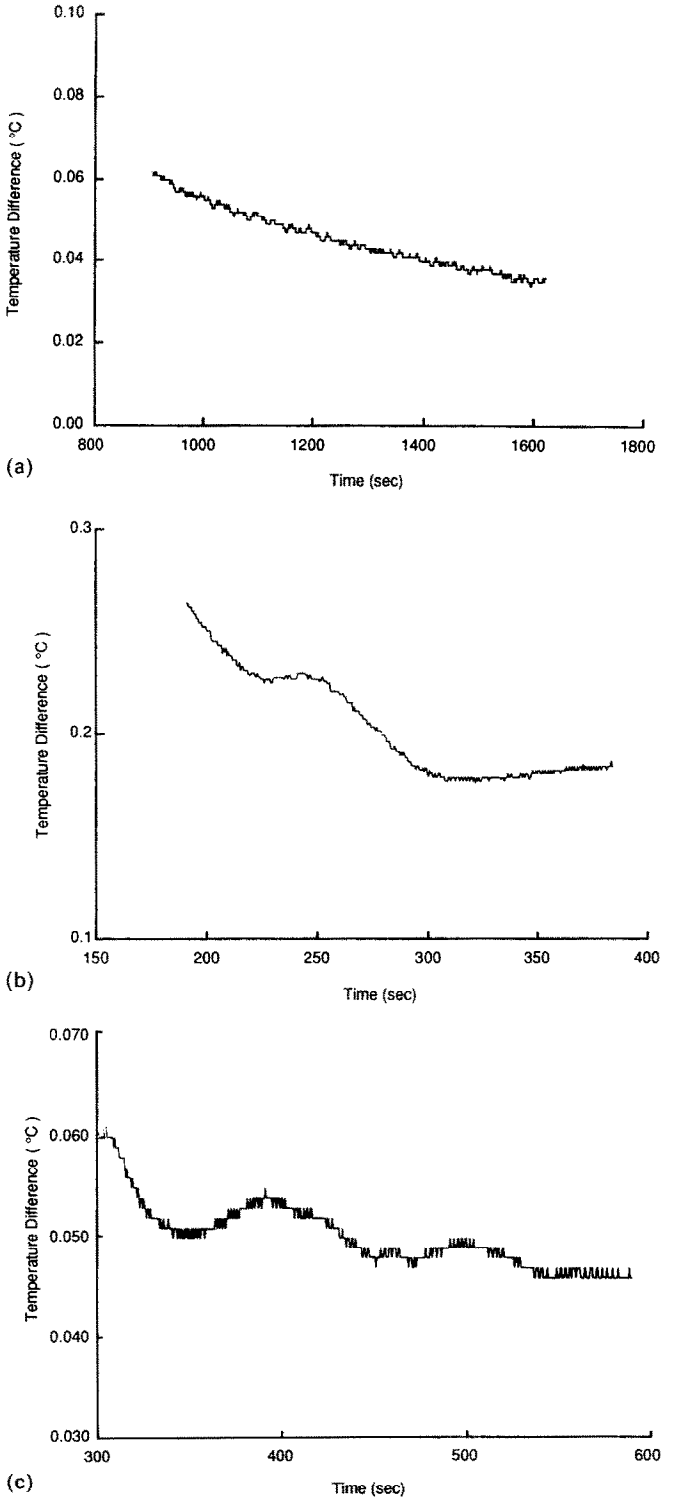

FIG. 8. Measured temperature difference between thermistors #3 and #5 drawn as a time series for experiments with: (a) $Pr = 234$, $Ra = 2.9 \times 10^7$; (b) $Pr = 83$, $Ra = 3.4 \times 10^8$; (c) $Pr = 13$, $Ra = 2.7 \times 10^8$.

boundary layer [12], the data is presented for the period following that impact. Consistent with the scaling, there is no evidence in the signal of an oscillatory component at any frequency.

Figure 8(b) shows the corresponding result for experiment 158; $Ra = 3.4 \times 10^8$, $Pr = 83$, which lies just inside Regime IV, with $Ra > Pr^4 A^{-4}$. Here a small amplitude oscillation is observed, heavily damped, consistent with the high Pr value. With a further increase in Ra relative to the lower boundary of Regime IV, the effect becomes even more pronounced. Figure 8(c) shows the temperature difference across the intrusion for experiment 249; $Ra = 2.7 \times 10^8$, $Pr = 13$. Although the amplitude is again small, the oscillation is clearly defined and survives for several periods. A similar result was also reported in refs. [11, 12] for $Ra = 3.26 \times 10^8$, $Pr = 7.5$. In common with that result, Fig. 8(c) also shows that the period of oscillation decreases with time; in the present case, the period is initially about 110 s, decreasing to 93 s. Experiments 181 and 245 give a similar result. These are not shown. In Figs. 8(a)–(c), the signals are highly amplified, and the high frequency signal observed in the figures is noise, fluctuating at the sampling frequency.

To obtain an order of magnitude estimate of the frequency of the observed wave, a linearly stratified core with a total vertical temperature difference of $2\Delta T$ was assumed [1]. This gave rise to an estimate of the frequency as

$$\omega = \frac{N}{(1+A^{-2})^{1/2}} \tag{13}$$

where the Brunt–Väisälä frequency N is defined by $N = (\nu\kappa\, Ra)^{1/2} h^{-2}$. The corresponding periods for experiments 181, 245, and 249, together with the case reported by Patterson [11], are shown in Table 2. Also shown in Table 2 are the observed initial periods of oscillation for these cases. In all cases, the observed period is substantially longer than the first mode oscillation period for the assumed linear stratification.

As discussed in ref. [10], the assumption of linear stratification is poor during the initial period of the flow development, when a three-layer structure, consisting of the two intrusions and a homogeneous core, is more appropriate. In that paper, the intrusions were assumed homogeneous, and the resulting eigenvalue problem for the internal waves was solved for a particular estimated intrusion thickness. This procedure gave close agreement for the early part of the oscillatory behaviour. Armfield and Patterson [10] hypothesized that as the cavity filled with heated and cooled fluid from the intrusions, the stratification approached the linear case, and the later part of the oscillatory period was well represented by the Patterson and Imberger [1] estimates.

A similar analysis has been performed with the present experimental data. Although the intrusion velocity was measured by the passage of the nose past the thermistors, the thickness cannot be accurately determined without vertical temperature profiles. With the velocity estimate, however, the thickness may be estimated from a knowledge of the flux exiting from the thermal boundary layer, given by equation (9). The numerical results of ref. [10] suggest that the appropriate constant for equation (9) is 2, so that

$$Q = 2\kappa\, Ra^{1/4}. \tag{14}$$

This allows an estimate of the intrusion thickness in each experimental case, the consistency of which is confirmed by comparison with the streak photographs. Furthermore, in the present case, the intrusions are assumed to be linearly stratified, resulting in a more accurate model than that reported in ref. [10] if the interior of the intrusion is approximately linearly stratified.

The results of the analysis are also shown in Table 2. The period predicted by this procedure (and the associated intrusion thickness on which it is based) are given, and clearly are in much better agreement with the early observed frequencies in every case, particularly as the oscillations become more clearly defined with increasing Ra.

CONCLUSIONS

The results of an experimental program to investigate the unsteady flow development in a cavity

Table 2. Estimated and observed values for the initial period of the first mode internal wave. The estimated periods are based on the ref. [1] scaling, and on the three-layer structure with the intrusion layer thickness shown in parentheses in each case

Exp. No.	Scaling estimate [s]	Observation [s]	Three-layer estimate [s]
181	53.0	95.0	101.0 (1.6 cm)
245	80.0	125.0	145.0 (1.5 cm)
249	67.0	110.0	115.0 (1.8 cm)
Patterson [11]	72.0	105.0	105.0 (2.0 cm)

resulting from the sudden heating and cooling of opposing sidewalls are reported here. The results are discussed in the context of the scaling arguments of ref. [1], and for the first time, give strong experimental support to several aspects of the scaling, over a range of parameter values which encompass three of the flow regimes defined by ref. [1].

In particular, the presence of the cavity scale seiching, observed numerically, has now been confirmed in Regime IV and above ($Ra > Pr^{4} A^{-4}$). Although the experimental results of refs. [11, 12] gave the first experimental observation of this for a single Ra value, the present results show the existence of the oscillation for a range of parameter values within the expected regime. To add further support, the results in Regime III do not show evidence of the oscillatory behaviour, as predicted in ref. [1].

The model of the thermal boundary layer development, on which the scaling in ref. [1] is based, is also supported by the thermistor data taken in the boundary layer. Here, the data confirm the existence of an initially conducting regime, with a growth timescale in excellent agreement with the scaling result. The viscous intrusion scaling is also supported by the experimental results.

It is therefore evident that the concept of the flow development described in ref. [1], and subsequently modified and expanded by refs. [8–10, 12] is substantially correct, although a number of issues remain to be investigated. Of particular interest in this regard are the questions of, first, the presence, or otherwise, of an overshoot in the thermal boundary layer growth as discussed in refs. [18, 19], and second, the presence, in some cases, of the travelling waves observed in the thermal boundary layer on initiation and on first impact of the incoming intrusion. The data discussed here indicate that in Regime III these travelling waves are not present on either initiation or impact of the intrusion, and further that only in the upper part of Regime IV are the waves unstable on the vertical boundary layer. The question of the role of these instabilities in the transition to periodic steady flow or to locally chaotic flow at higher Ra remains to be answered.

Acknowledgement—This research was supported by the Australian Research Council under grant No. A48615453. The authors acknowledge many useful discussions with Dr S. W. Armfield and his and Dr S. G. Schladow's comments on an earlier draft of the manuscript.

REFERENCES

1. J. C. Patterson and J. Imberger, Unsteady natural convection in a rectangular cavity, *J. Fluid Mech.* **100,** 65–86 (1980).
2. P. M. Gresho, R. L. Lee, S. T. Chan and R. L. Sani, Solution of the time-dependent incompressible Navier–Stokes equations using Galerkin finite difference method. In *Approximation Methods for Navier–Stokes Problems*, Springer Lecture Notes in Mathematics No. 771, pp. 203–222. Springer, Berlin (1980).
3. B. Staehle and E. Hahne, Overshooting and damped oscillations in transient natural convection flows in cavities, *Proc. 7th Int. Heat Transfer Conf.*, Munich (1982).
4. P. Yewell, D. Poulikakos and A. Bejan, Transient natural convection experiments in shallow enclosures, *Trans. ASME*, Ser. C, *J. Heat Transfer* **104,** 533–538 (1982).
5. J. C. Patterson, On the existence of an oscillatory approach to steady natural convection in cavities, *J. Heat Transfer* **106,** 104–108 (1984).
6. G. N. Ivey, Experiments on transient natural convection in a cavity, *J. Fluid Mech.* **144,** 389–401 (1984).
7. S. Paolucci and D. R. Chenoweth, Transition to chaos in a differentially heated vertical cavity, *J. Fluid Mech.* **201,** 379–410 (1989).
8. S. G. Schladow, J. C. Patterson and R. L. Street, Transient flow in a side-heated cavity at high Rayleigh number: a numerical study, *J. Fluid Mech.* **200,** 121–148 (1989).
9. S. G. Schladow, Oscillatory motion in a side heated cavity, *J. Fluid Mech.* **213,** 589–610 (1990).
10. S. W. Armfield and J. C. Patterson, Direct simulation of wave interactions in unsteady natural convection in a cavity, *Int. J. Heat Mass Transfer* **34,** 929–940 (1991).
11. J. C. Patterson, Experiments in unsteady natural convection, *Conf. Proc. Fourth Australasian Conf. on Heat and Mass Transfer, Heat and Mass Transfer '89*, University of Canterbury, Christchurch, New Zealand, pp. 299–306 (1989).
12. J. C. Patterson and S. W. Armfield, Transient features of natural convection in a cavity, *J. Fluid Mech.* **219,** 469–497 (1990).
13. S. W. Armfield, Finite difference solution of the Navier–Stokes equations on staggered and non-staggered grids, *Computers Fluids* **20,** 1–17 (1991).
14. J. M. Hyun and J. W. Lee, Numerical solutions for transient natural convection in a square cavity with different sidewall temperatures, *Int. J. Heat Fluid Flow*, **10,** 146–151 (1989).
15. J. B. Segur, Physical properties of glycerol and its solutions. In *Glycerol* (Edited by C. S. Miner and N. N. Dalton). Reinhold, New York (1953).
16. S. N. Brown and N. Riley, Flow past a suddenly heated vertical plate, *J. Fluid Mech.* **59,** 225–237 (1973).
17. A. E. Gill and A. Davey, Instabilities of a buoyancy-driven system, *J. Fluid Mech.* **35,** 775–798 (1969).
18. J. C. Williams, J. C. Mulligan and T. B. Rhyne, Semi-similar solutions for unsteady free-convective boundary-layer flow on a vertical flat plate, *J. Fluid Mech.* **175,** 309–332 (1987).
19. R. J. Goldstein and D. G. Briggs, Transient free convection about vertical plates and circular cylinders, *J. Heat Transfer* **86,** 490–500 (1964).

ETUDE EXPERIMENTALE DE LA CONVECTION NATURELLE VARIABLE DES MELANGES GLYCEROL–EAU DANS UNE CAVITE CHAUFFEE LATERALEMENT

Résumé—On donne les résultats d'expériences conduites dans une cavité carrée brusquement chauffée et refroidie sur les faces latérales opposées. Le fluide de travail initialement stationnaire et isotherme est un mélange glycérol–eau donnant un nombre de Prandtl variable entre 13 et 234. Ce domaine, allié à une variation de la différence de température de bout en bout, conduit à une exploration avec une transition monotone–oscillatoire pour l'approche de l'état stationnaire prédite par Patterson et Imberger (*J. Fluid Mech.* **100**, 65–86 (1980)). Les résultats confirment leur classification et d'autres aspects du développement de l'écoulement, incluant les caractéristiques de la croissance des couches limites thermique et quelques caractéristiques des intrusions horizontales depuis les couches thermiques dans la cavité.

EXPERIMENTELLE UNTERSUCHUNG DER TRANSIENTEN NATÜRLICHEN KONVEKTION VON GLYZERIN/WASSER-GEMISCHEN IN EINEM SEITLICH BEHEIZTEN HOHLRAUM

Zusammenfassung—Es wird über Versuchsergebnisse berichtet, die in einem quadratischen Hohlraum bei plötzlicher Beheizung und Kühlung an gegenüberliegenden Seitenwänden ermittelt wurden. Das Arbeitsfluid ist in allen Fällen ein Glyzerin/Wasser-Gemisch, das zu Beginn in Ruhe und isotherm ist, und das Variationen der Prandtl-Zahl im Bereich 13–234 ermöglicht. Zusammen mit einer Variation der Temperaturdifferenz zwischen den Endflächen gestattet dieser Bereich die Ermittlung des Parameterraumes, in dem der Übergang von einer monotonen zu einer oszillierenden Annäherung an den stationären Zustand durch das klassische Verfahren von Patterson und Imberger (*J. Fluid Mech.* **100**, 65–86 (1980)) vorhergesagt wird. Die Ergebnisse bestätigen die Klassifizierung und andere Aspekte der Strömungsentwicklung. Darunter wird beispielsweise die Charakteristik des Wachstums der thermischen Grenzschichten und einige Eigenheiten des waagerechten Einbringens der thermischen Schichten in den Hohlraum verstanden.

ЭКСПЕРИМЕНТАЛЬНОЕ ИССЛЕДОВАНИЕ НЕСТАЦИОНАРНОЙ ЕСТЕСТВЕННОЙ КОНВЕКЦИИ СМЕСЕЙ ГЛИЦЕРИНА И ВОДЫ В ПОЛОСТИ С БОКОВЫМ НАГРЕВОМ

Аннотация—Проведен ряд экспериментов в квадратной полости с внезапным нагревом и охлаждением на противоположных боковых стенках. Во всех случаях в качестве рабочей жидкости, находившейся в начальный момент времени в изотермических условиях, использовалась смесь глицерин-вода, число Прандтля которой изменялось в диапазоне 13–234. В указанном диапазоне при изменяющейся разности температур на торцах исследовалась область параметров, в которой переход от монотонного к колебательному режиму приближения к стационарному состоянию определяется по классификационной схеме Паттерсона и Имбергера (*J. Fluid Mech.* **100**, 65–86 (1980)). Полученные результаты подтверждают правомерность этой классификации, а также другие аспекты развития течения, включая характеристики роста тепловых пограничных слоев и некоторые характеристики горизонтальных интрузий из тепловых слоев в полость.